UNIVERSITY OF CALGARY

Energy & Environmental Systems EES iseee

Energy and Environmental Systems Group

Institute for Sustainable Energy, Environment and Economy (ISEEE)

Reservoir Modelling

Wabamun Area CO_2 Sequestration Project (WASP)

Authors

Seyyed Ghaderi

Yuri Leonenko

Rev.	Date	Description	Prepared by
1	August 14, 2009	First draft	Yuri Seyyed
2	August 19, 2009	Revision	Yuri Seyyed

Table of Contents

INTRODUCTION 5

DISCUSSION 5

1. NUMERICAL RESERVOIR MODELLING 5
   1.1. Preliminary Conceptual Model 5
   1.2. Detailed Model with Full Aquifer (Nisku) Extent 9

2. LONG-TERM FATE OF CO_2 17
   2.1. Pressure Field Evolution During and After Injection Until Initial Reservoir Pressure Reached 17
   2.2. Effect of Aquifer Dip on Plume Movement and Size 18
   2.3. Estimation of Timescale for Free-Phase CO_2 after Injection (onset and dissolution time for natural convection scenario) 18

3. INVESTIGATION OF THE PHASE BEHAVIOR OF H_2S SATURATED BRINE IN CO_2 SEQUESTRATION PROCESS 19
   3.1. Fluid Representation of CO_2-Brine and CO_2-H_2S-Brine Systems 19
   3.2. Description of the Simulation Model 20
   3.3. General Simulation Results 20
   3.4. Base Case Simulation Results and Observations 22
   3.5. Sensitivity Analysis 23

SUMMARY 26

ACKNOWLEDGMENTS 26

REFERENCES 27

List of Tables

Table 1: Reservoir properties. 6

List of Figures

Figure 1: Nisku relative permeability curves. 6
Figure 2: Configuration of injection wells and element of symmetry (salmon area). 7
Figure 3: Effect of different parameters on storage capacity: a) effect of distance between wells, b) effect of compressibility, c) effect of permeability, d) effect of aquifer thickness. 8
Figure 4: Top view of the Nisku formation in the Wabamun Lake area (left), study area is outlined in red and base formation/properties used are shown on the right. 10
Figure 5: Plume extension (top row) and pressure radius of investigation (bottom row) after 50 years of injection for different wells in the Nisku study area (within the red area in Figure 4) 10
Figure 6: Pressure evolution: left, one well; right, 10 wells. 11
Figure 7: Variation of Nisku capacity with respect to number of wells and formation properties (red curve represents base properties). 12
Figure 8: Pressure at the end of injection. 12
Figure 9: Comparison of the effect of different well orientations and stimulation on the storage capacity of the model. 13
Figure 10: Five geo-statistical realizations for porosity and permeability. 14
Figure 11: Object-based realization of porosity. 14
Figure 12: Saturation (left) and pressure (right) fields for stochastic modelling after 50 years of injection. 15
Figure 13: Injection capacity for five realizations. 15
Figure 14: Injection capacity for different fracture pressures. 15
Figure 15: Saturation (left) and pressure (right) fields for object-based modelling after 50 years of injection. 16
Figure 16: Injection capacity for object-based modelling. 16
Figure 17: Pressure evolution (each well injects 0.5 Mt/year for 50 years). 17
Figure 19: Saturation field for a single injector: a) base properties; b) permeability is increased to 150 mD. 18
Figure 20: Short-term (a) and long-term (b) processes involved in geological storage. 19
Figure 21: Water-gas relative permeability curves. 20
Figure 22: Variation of gas saturation around the injection well after 200 days. 21

INTRODUCTION

Although it is recognized that deep aquifers offer the potential for very large storage capacities for CO_2 sequestration, it is not clear what the best method is to fill these aquifers with large volumes of CO_2 in a relatively short period of time within localized injection areas. The typical benchmark for the rate of CO_2 injection is 1 Mt/year when studying storage performance. This rate is very low when compared to the scale needed for storage technology to play a significant role in managing global emissions. In this report we study the feasibility of injecting large volumes of CO_2 into the Nisku aquifer, which is located in the Wabamun Lake area in Alberta, Canada *[1]*. In this area, large CO_2 emitters include four coal-fired power plants with emissions that range between 3 and 6 Mt/year each, which together emit ~ 20 Mt/y or ~ 1 Gt over 50 years. This number, 1 Gt, is considered the target capacity for WASP. The Nisku aquifer is believed to be a suitable choice for future sequestration projects. The main objectives of the WASP study are as follows.

i) *Estimate storage capacity*. Traditionally, storage capacity is determined by available pore space. For this study a more practical aspect was used—the maximum amount that can be injected within a short period of time (~ 50 years) within a localized injection area (~ 30 km × 90 km). The capacity of individual reservoirs to accommodate large injection volumes should be evaluated by assessing the ability to inject CO_2 without exceeding formation fracture pressures. A number of options were also considered to increase storage capacity.

ii) *Determine CO_2 plume movement and pressure distribution.* These factors were determined for the period during and after injection. The shape and dip of the aquifer, the number of wells and their placement (among other parameters) would be considered.

iii) *Estimate long-term fate of injected CO_2.* Estimate the timescale for the long-term fate of the injected CO_2 associated with free-phase CO_2, aquifer pressurization, and the effect of dip on plume shape and its migration.

iv) *Investigate phase behaviour*. Investigate the phase behaviour of H_2S initially saturated in brine in the CO_2 sequestration process.

DISCUSSION

1. NUMERICAL RESERVOIR MODELLING

1.1. Preliminary Conceptual Model

To develop a benchmark at the beginning of the project, a simplified conceptual model was developed based on homogeneous properties and an infinite acting aquifer. The properties for the simulations were taken from Hitchon, 1996 *[1]* (Table 1). The table data was then revised using WASP preliminary analysis data: permeability was changed to 30 md, porosity to 10%, aquifer thickness to 70 m and PVT table for density and viscosity were generated based on Hassanzadek et al, 2008 *[2]*. The relative permeability curves (Figure 1) were taken from literature (Bennion and Bachu, 2005 *[3]*).

Table 1: Reservoir properties.

Description	Result
Depth (m)	1860
Thickness (m)	70
Pressure at aquifer top (MPa)	16
Temperature (°C)	60
Permeability (md)	6.2 – 400
Vertical anisotropy	0.27
Porosity (%)	6 – 12
Salinity of formation water (mg/l)	190000
Density of formation water (kg/m^3)	1155.5
Viscosity of formation water (mPa.s)	0.840

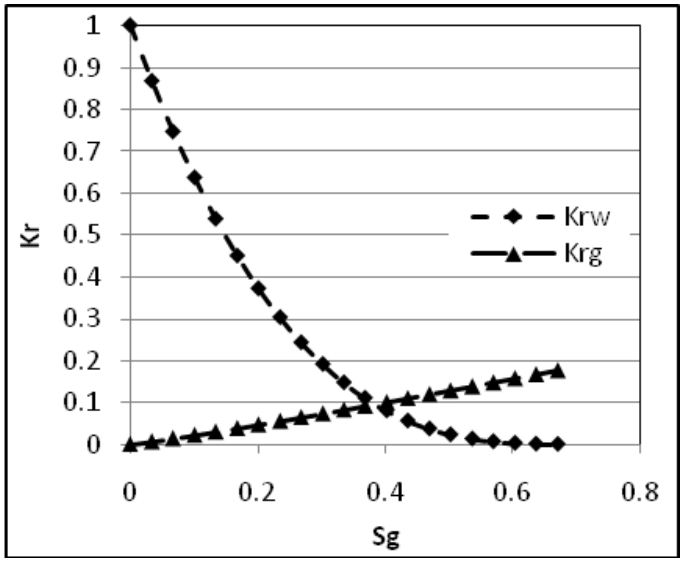

Figure 1: Nisku relative permeability curves.

For this model, a square (200 km × 200 km) simulation domain was chosen to represent an aquifer (the results were not sensitive to an increase in model size to 250 km × 250 km). By setting the model to these dimensions, the aquifer behaves as though it is infinite acting for the injection of the target volume of CO_2.

Figure 2 shows the model configuration for the different numbers of vertical injector wells, starting with 1 and ending with 25. All wells are perforated from the top to the bottom of the aquifer. The number of wells (n) was chosen to allow the use of an element of symmetry and hence reduce the total number of grid cells by a factor of four. The distance between the wells in both the x and y directions are the same and equal to λ. The total cumulative amounts of injected CO_2 (Q1, Q4, Q9, Q16 and Q25) increase with the number of wells, and these amounts are split equally between injectors in each case. For example in the case of 16 wells, the flow rate per well is Q16/(16 wells × 50 years).

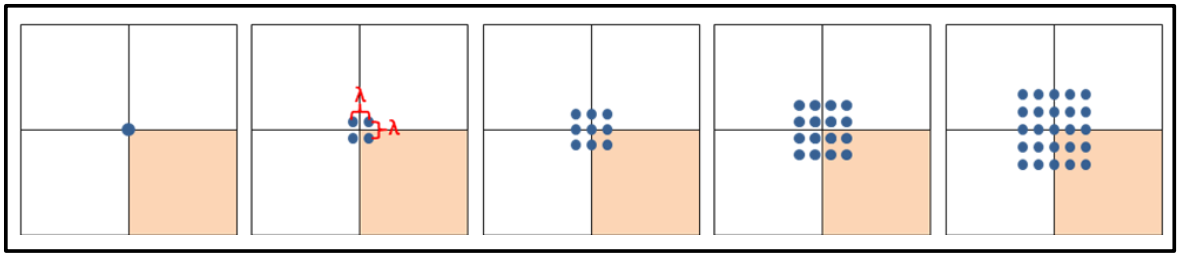

Figure 2: Configuration of injection wells and element of symmetry (salmon area).

Single Injector (capacity and plume size)

The saturation and pressure fields for a single well, as well as for multiple injection scenarios, will be shown in the following section (Section 1.2, Detailed Model with Full Aquifer Extent), since the results are very similar. A brief summary for a single injector:

- plume radius after 100 years of simulation is ~ 4.6 km; and
- capacity of one vertical well is ~ 1 Mt/y (based on P_f = 40 MPa), horizontal well improves capacity with a maximum rate of ~ 1.5 Mt/y. (The value for the fracture pressure will be discussed later in this report.)

Multiple Injectors

For multiple (n>1) injection scenarios, CO_2 saturation plumes have no interference and n individual plumes have a radius of 4 to 5 km for each injector.

The pressure field behaves totally different than the saturation field. By the fiftieth (50^{th}) year of CO_2 injection, there are no individual pressure plumes. Instead, most of the pressure plumes have merged into a single large (scale of hundred km) pressure disturbance. Injection capacity increases with the number of wells, but there is limited benefit to adding incremental wells after 15 to 20. These phenomena will be discussed in detail in Section 1.2 when more advanced modelling for the Nisku aquifer is considered.

Sensitivity of Injectivity to Different Reservoir Properties (permeability, rock compressibility, aquifer depth) and Well Placement (generic study)

The sensitivity study in this section was performed using generic variables. The properties of the reservoir were chosen similarly to those used in the Berkeley Laboratory inter-comparison study *[4]*. This study and its properties are well known, so they could be used as a benchmark for representative aquifers for generic studies. The aquifer is considered to be homogenous, isotropic, and isothermal with a thickness of 100 m and permeability of 1.0×10^{-13} m^2 (100 mD), porosity is 12%, rock compressibility of 4.5×10^{-10} 1/Pa, and fracture pressure equal to 30,000 kPa. In all runs, the initial conditions include a temperature of 45°C, pressure of 12000 kPa, salinity of 15% of NaCl by weight, brine saturation of 1, and gas saturation of zero. All simulation runs involve continuous injection for 50 years. Bottom hole injection pressure is monitored and constrained to less than 27 MPa over the entire injection period. These parameters define a maximum CO_2 storage capacity over a period of 50 years.

Figure 3-a shows the storage capacity considering the number of vertical wells and the distance between them. As this figure indicates, the required number of wells to achieve the target volume (1 Gt of total injection) is 25 situated 8 km apart. For practical reasons it may be better to use a smaller or larger number of wells covering a larger or smaller area. Extrapolating the green and red curves, we can roughly estimate the number of wells required. For example, 18 wells that are 10 km

apart or 28 wells that are 6 km apart will achieve the same target (although in these cases the placement will not be symmetrical and new simulations will have to be performed). With respect to the area of injection, there would be no preference between these three choices (6 km, 8 km or 10 km well separation). For sensitivity analysis, the blue curve in Figure 3-a corresponds to 25 wells that are 8 km apart. This will be used as the base case for the sensitivity study, and all other data will be compared to it. The case covers an area of 1024 km^2 (32 km $\times$ 32 km), which is a considerably large area. As the number of wells increase, the injection rate of each well decreases to compensate for the excess pressure build-up associated with new wells that affect the pressure response of the central wells. Hence, the initial steep slope of the graphs (from 1 to 4 wells) quickly approaches a constant slope.

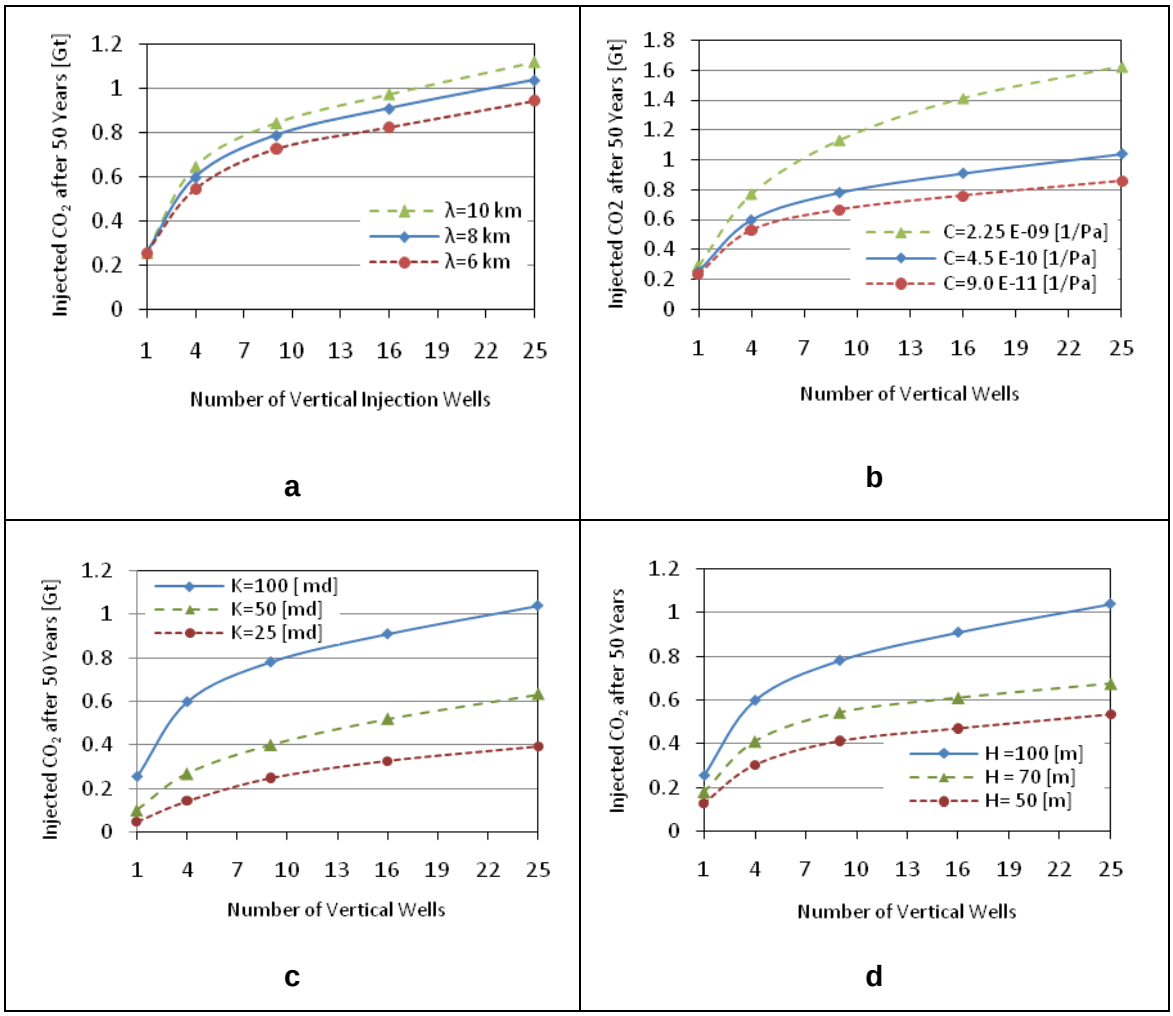

Figure 3: Effect of different parameters on storage capacity: a) effect of distance between wells, b) effect of compressibility, c) effect of permeability, d) effect of aquifer thickness.

Additional simulations were conducted to investigate the effect of some aquifer properties, such as rock compressibility, absolute permeability and thickness (Figures 3-b, 3-c and 3-d), on the amount of injected and stored CO_2 after 50 years. Since for the base case properties it was possible to inject the desired value of 1 Gt CO_2 over 50 years, the values for the parameters for the other scenarios were chosen closer to the expected aquifer properties. In all cases, the rates of CO_2 injection were

adjusted such that at the end of injection period, the maximum bottom-hole pressure reached the highest sustainable pressure.

Depending on the rock composition of the formations, the compressibility of the reservoirs varies widely. Hence for sensitivity study, the value of compressibility was varied within one order of magnitude by multiplying and dividing the base case value by five, respectively. Figure 3-b shows the outcome. Higher values of compressibility cause significant differences on the results, especially when the number of well increases.

The permeability of the formation controls both the pressure distribution over the system volume and the propagation velocity of the pressure pulse away from the injection site. According to the diffusivity equation, pressure will diffuse faster in formations with higher permeability or lower compressibility. Although it is quite possible to find localized regions with high absolute permeability within an aquifer (which are usually allocated to injection sites), generally the average permeability of the formation may be low. Figure 3-c depicts the results of simulations for different values of permeability. As the permeability is reduced by half, the amount of stored CO_2 nearly decreases by half. By reducing the permeability, the initial steep slope of the previous curves decreases. This illustrates that increasing the number of wells does not contribute significantly to capacity in low permeable formations.

The last parameter considered was the thickness of the formation. Reducing the thickness by 50% of the initial value has almost the same effect as reducing the absolute permeability by half (as would be anticipated). Figure 3-d indicates that for thinner reservoirs, more wells should be placed in the injection zone or other methods for increasing injectivity should be considered.

1.2. Detailed Model with Full Aquifer (Nisku) Extent

In the following section, the simulation results for CO_2 injection in the Nisku formation will be presented. First, a homogenous model is used to investigate the performance of a semi-infinite formation on injectivity. Then a heterogeneous model is populated with realistic permeability and porosity fields in order to demonstrate the effect of heterogeneity and reservoir dip angle on the evolution of a CO_2 plume and the associated impact on reservoir pressure.

Development of Full Aquifer Extent Geometry

Figure 4 shows the top view of the Nisku aquifer. The region covers an area of about 450 km × 640 km, while the bounded area by the red line shows the focus injection area. The majority of core and log data are related to available wells in this area and the injection site will be confined within this boundary. The area of this focus region is approximately 1500 km^2. The thickness of the numerical model is 70 m. Thirty layers with variable thickness are used to create the 3D model. The base properties used are the same as for the conceptual model.

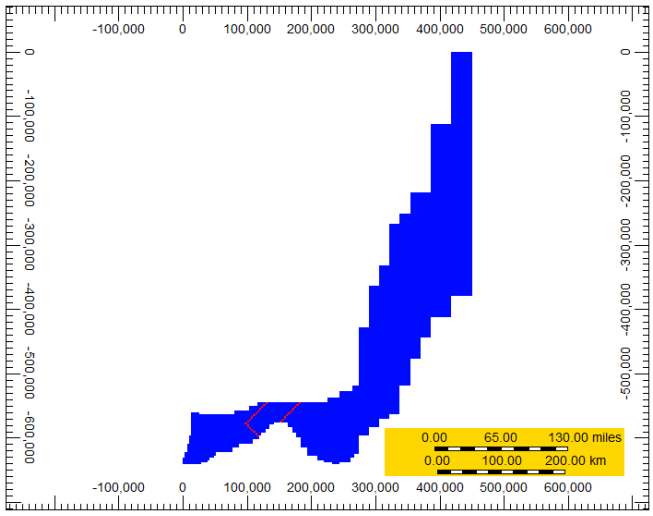

Properties Used as a Base	
Depth	1860 m
Thickness	70 m
Temperature	60°C
Permeability	30 mD
Porosity	10%
Salinity	190,000 mg/l
Rock Compressibility	4.5×10^{-7} 1/KPa

Figure 4: Top view of the Nisku formation in the Wabamun Lake area (left), study area is outlined in red and base formation/properties used are shown on the right.

Plume Size and Pressure Field Depending on Number of Injectors

Figure 5 presents the plume extension and pressure distribution after 50 years of injection using the base case properties. For the case with one well, the plume radius at the top layer is about 4.6 km, which is consistent with the conceptual model as well as the analytical solution radius *[5]*. It is noticeable that the size of the "*pressure plume*" is much larger at about 65 km, even for one well. In the cases of *n* number of injectors, one can see *n* individual plumes for CO_2 saturation. As the number of wells increase, the individual injector flow rate decreases (fracture pressure constraint) and consequently the plume radius decreases. However for pressure, one can see a very strong interference between injectors that pressurizes the total area of injection. The pressure build-ups and soon merges, and thereafter a cumulative pressure disturbance dissipates radially away from a central position, which is the well position for one well model and is near the centre of the focus area for the models.

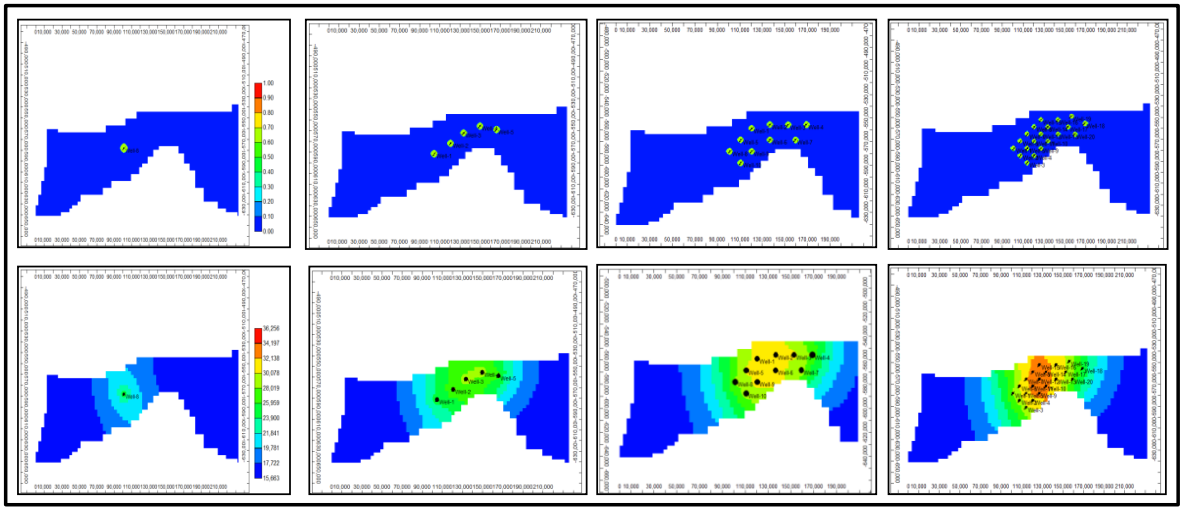

Figure 5: Plume extension (top row) and pressure radius of investigation (bottom row) after 50 years of injection for different wells in the Nisku study area (within the red area in Figure 4)

It is very important to mention that the dynamics of the pressure field is very different for one injection well, Figure 6 left, than for multiple injection wells, Figure 6 right.

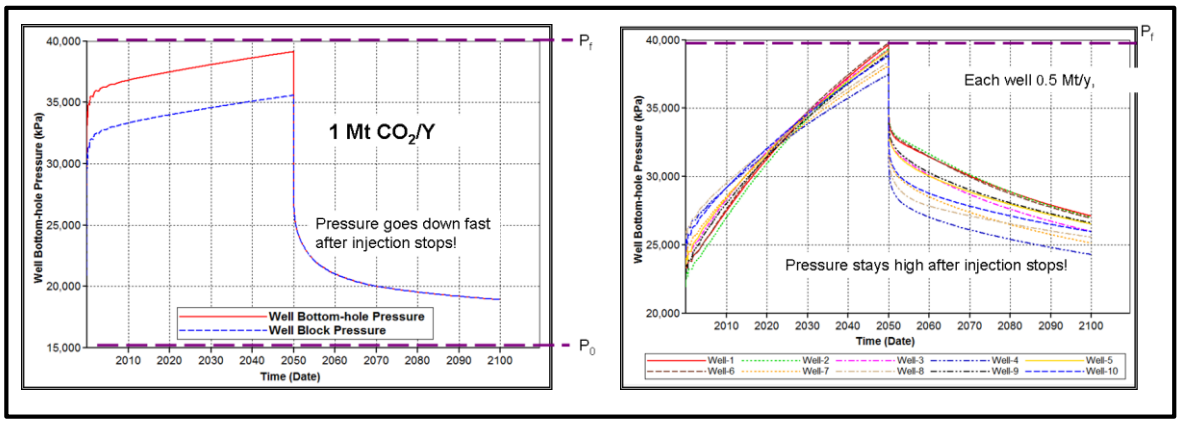

Figure 6: Pressure evolution: left, one well; right, 10 wells.

One can see that the pressure fall-off after ending CO_2 injection is much quicker for a single well. The pressure fall-off for multiple wells is delayed because of the larger pressure influence area.

Injection Capacity (versus number of wells and its sensitivity to different properties)

Starting with one well, the maximum achievable rate was determined to be as high as 1.1 Mt CO_2/year (matching the results of the conceptual model), which is equivalent to 0.055 Gt after 50 years. This flow rate causes the bottomhole pressure to reach 40 MPa at the end of the injection period. This value was assumed by the WASP team at the beginning of the project based on some literature data for Alberta reservoirs. Midway through the project, the Geomechanical Simulation Group estimated this value to be around 35 to 37 MPa. Since our original assumption was very close to the new calculated value (which is not based on real field data), we decided to keep 40 MPa in our reservoir model. The sensitivity of capacity to different fracture pressure (within the range 30 to 40 MPa) is presented later in this section. Also there is discussion (in the Geomechanical Simulation Group Report) of the impact of pressure difference on fracture pressure during injection.

When the next five wells are placed in the zone, the corresponding flow rate for each well is reduced to 0.625 Mt/year per well with cumulative injection of 0.15 Gt. Increasing the number of wells to 10 brings the flow rate to 0.418 Mt/year per well with total injected CO_2 of 0.209 Gt. Finally, the values for 20 wells are equal to 0.238 Mt/year and 0.238 Gt, respectively. These results are shown in Figure 7, red curve. We also determined what reservoir properties we would need to achieve the target of 1 Gt. The green curve on Figure 7 presents the injection capacity of the focus area with the following aquifer properties: porosity 20% and horizontal permeability 90.0 (mD). Although these values caused a significant difference in the outcome, the limitation in injectivity improvement for more than 10 wells still existed. It could not be claimed that these values are the maximum injectivity and storage of the formation because no optimization with respect to well positioning and flow rate was performed.

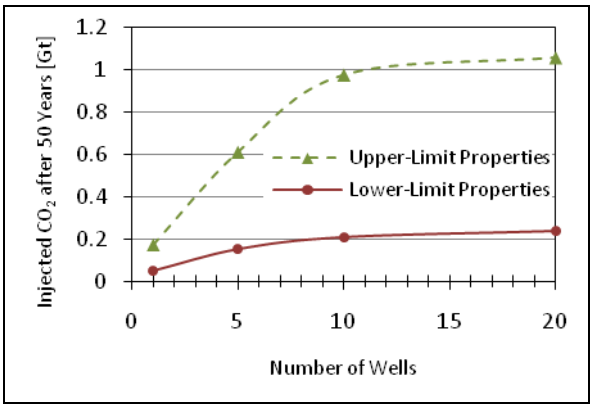

Figure 7: Variation of Nisku capacity with respect to number of wells and formation properties (red curve represents base properties).

Some Options to Increase Capacity (horizontal injection, fracturing)

In the storage process the term "capacity" could have two meanings. The apparent capacity is the available and accessible pore volume of the aquifer, and the injection capacity is the amount of CO_2 that can be realistically injected into the formation and is a function of the number of wells and the fracture pressure of the formation and the confining caprock *[6]*. As discussed earlier, for a restricted injection area such as in the Nisku study, increasing the number wells beyond a certain limit (which is controlled by formation properties and injection site area) has a minor effect on the injection capacity. The focus of this section is to investigate methods that lead to an increase in injection capacity in the aquifer.

The first method is to use horizontal wells instead of vertical wells. For vertical wells, it is preferable to use fully penetrated wells over the entire thickness of the aquifer. To find the minimum length for a horizontal well, the effective radius of pressure disturbance around the vertical injection well, which is again a function of formation properties, should be determined. For vertical wells, as the injection begins the pressure around the wellbore increases rapidly and causes the development of locally narrow width pressure peaks in the vicinity of the well, Figure 8.

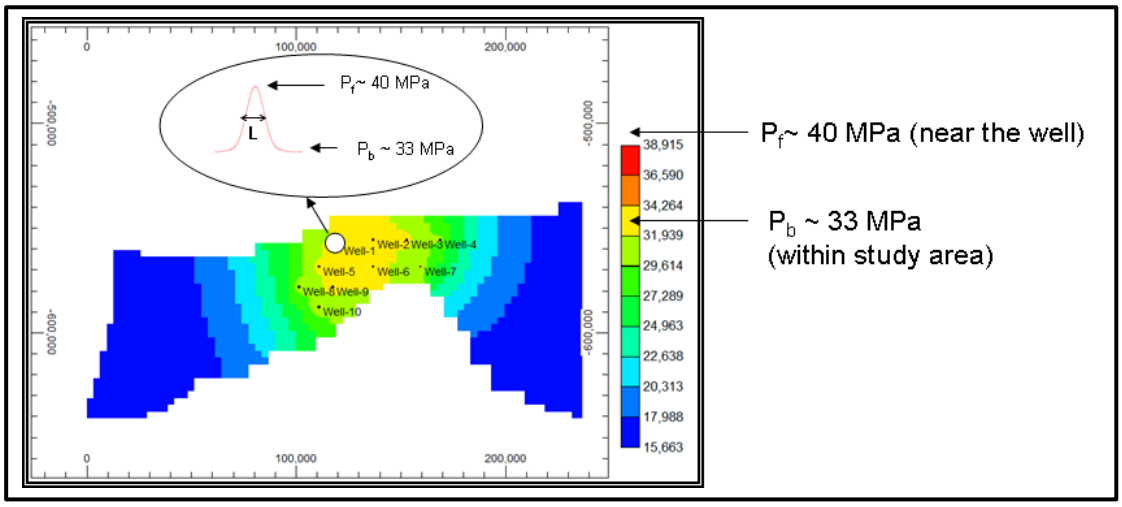

Figure 8: Pressure at the end of injection.

Using horizontal wells with total length greater than the scale of the vertical injection well's pressure peak "*L*" (for the Nisku formation this minimum required well was estimated to be equal to 3000 m) will diminish these peaks and increase injectivity, Figure 9 (H-Well Bar). The V-Well Bar corresponds to vertical injectors.

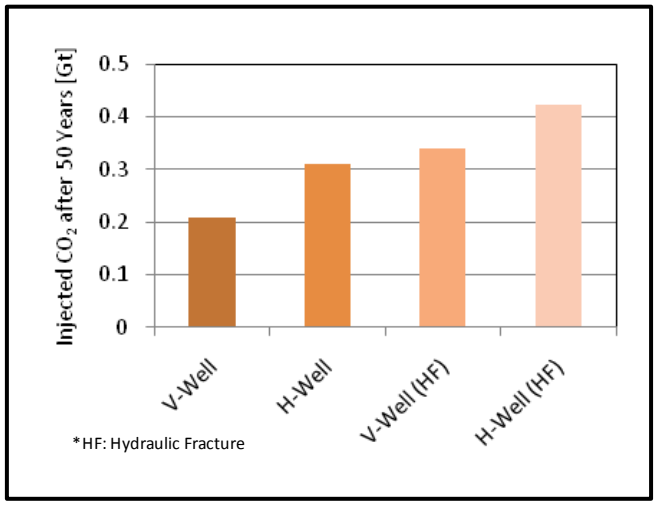

Figure 9: Comparison of the effect of different well orientations and stimulation on the storage capacity of the model.

The application of stimulation techniques, such as hydraulic fracturing, can improve injectivity as long as the caprock is not fractured. The technical feasibility of implementing these techniques requires careful geomechanical characterization of the formation. Vertical wells with hydraulic fractures were modelled by constructing thin grid blocks 400 m (fracture half length) from the well grid toward the east and west. A porosity of 0.15 and permeability of 1500 mD were assigned to these grid blocks to approximate a 400 m half-length fracture and associated damage zone. These properties were also used to construct four 100 m half lengths of four staggered hydraulic fractures for the horizontal wells. The V-Well (HF) and H-Well (HF) bars in Figure 9 shows the simulation results for 10-wells cases (located as in Figure 8) in the Nisku aquifer (V = vertical wells, H = horizontal). Another promising method of increasing CO_2 capacity would be to produce the brine *[7]* from the formation to prevent the reservoir pressure from building up excessively near the injection wells. This method involves transporting produced brine through surface pipelines to a location where the brine can be injected into another compatible formation or into a lower pressure region of the Nisku aquifer itself.

Heterogeneity Sensitivity Study

Two kinds of heterogeneity were considered in this study: stochastic and object-based models. The stochastic model was based on existing quantitative data (i.e., wireline log, acoustic impedance) and geostatistical tools. It relies on resistivity-derived porosities and permeabilities from nearly 60 wells. For this study, five equiprobable realizations of properties (porosity, %: max-28.6, min-1.3, mean-4.9) and (permeability, mD: min-3.1; max-393; mean-22.37) were generated, see Figure 10. All sets of realizations for this section (heterogeneity sensitivity study) were developed by the geostatistics group and the detailed description of these realizations and the methodology is presented in the Geomodelling Section of this report, which was written by Chris Eisinger and Jerry Jensen.

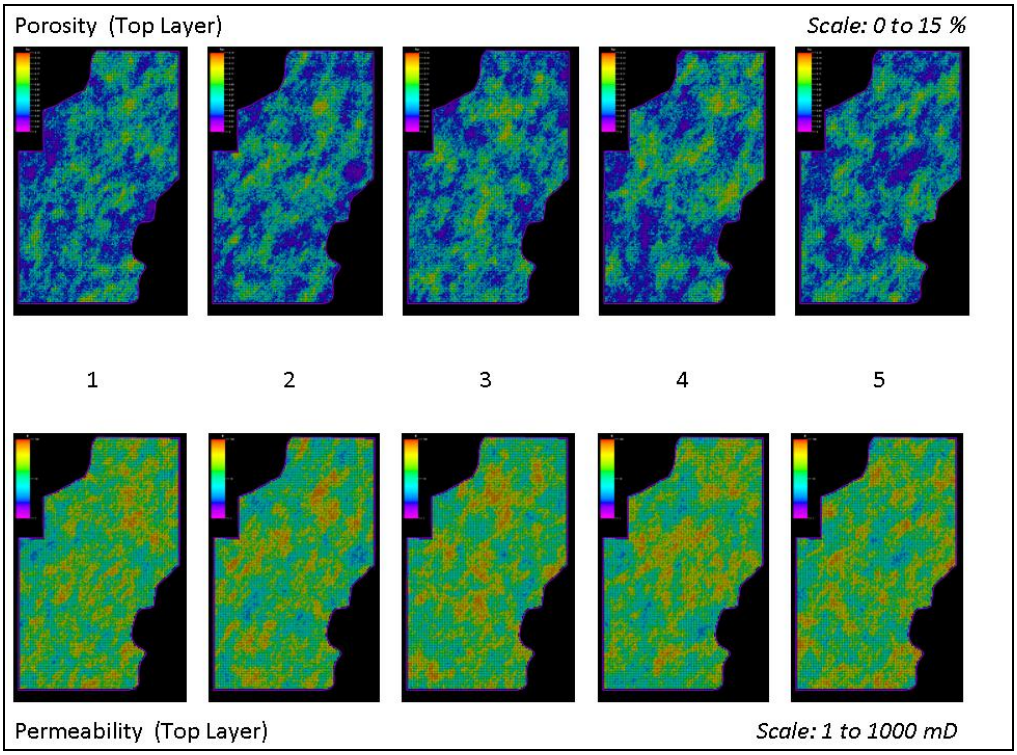

Figure 10: Five geo-statistical realizations for porosity and permeability.

Object-based models define "objects" (same sizes) as higher porosity and permeability zones, the geometry and distribution which are constrained by dimensions of existing modern carbonate analogs, conceptual understanding of Nisku carbonate in the Wabamun area, wireline log data and seismic data.

Two kinds of objects: i) dark blue (Minor width-500 m, Major/Minor ratio -5 and Thickness -5 m) and ii) light blue (Minor width-300 m, Major/Minor ratio -5 and Thickness -2 m) all oriented along the dip were distributed in each zone (upper, middle, and lower, see Figure 11 left) of the Nisku open marine. Figure 11 right (Upper third has 13 layers with average vertical grid size z = 1.72 m; Middle third has 5 layers with z = 4.46 m and Lower third has 12 layers with average z = 1.86 m).

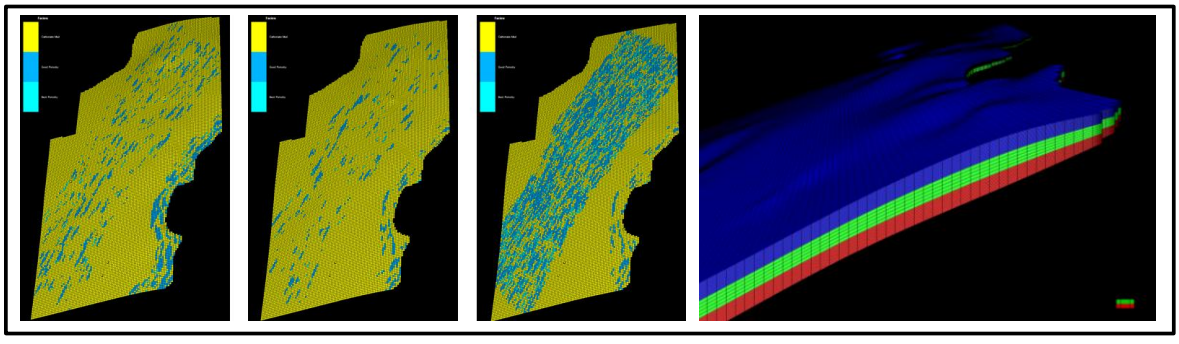

Figure 11: Object-based realization of porosity.

For the stochastic modelling examples (realizations 4 and 5), the saturation and pressure fields are shown in Figure 12.

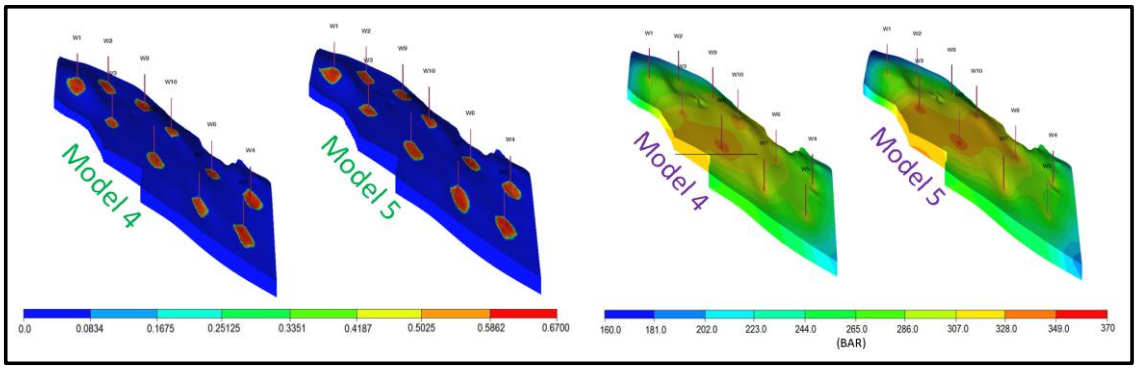

Figure 12: Saturation (left) and pressure (right) fields for stochastic modelling after 50 years of injection.

Although one can see some differences on a small scale for both fields, the injection capacities for all cases are almost identical (Figure 13), and very close to being homogeneous (Figure 7 for 10-well injection).

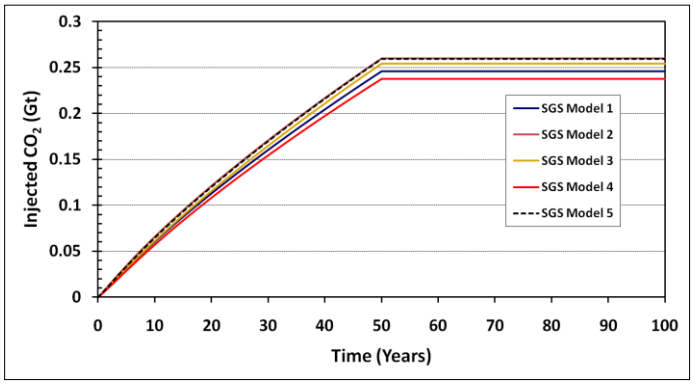

Figure 13: Injection capacity for five realizations.

The above results represent the storage capacity when the fracture pressure was set to 40 MPa. Sensitivity of capacity to fracture pressure is shown in Figure 14.

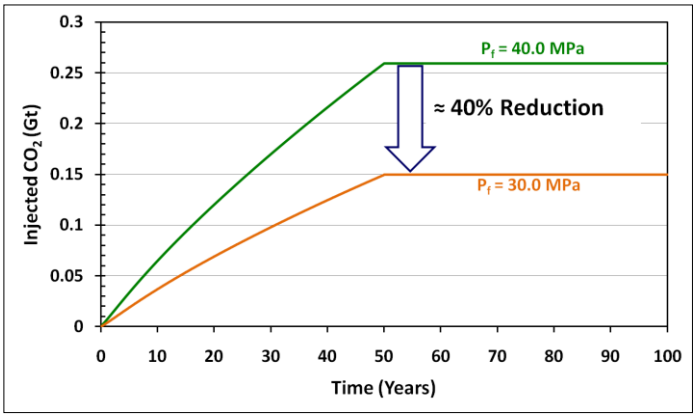

Figure 14: Injection capacity for different fracture pressures.

For object-based modelling, the saturation and pressure fields are shown in Figure 15.

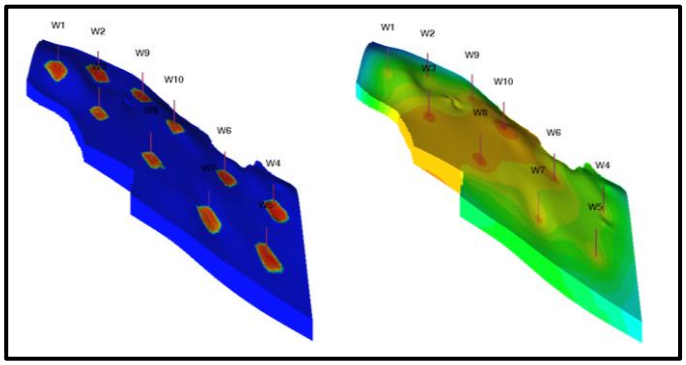

Figure 15: Saturation (left) and pressure (right) fields for object-based modelling after 50 years of injection.

Injection capacity, as in the case of stochastic modelling, is very close to the homogeneous model, see Figure 16.

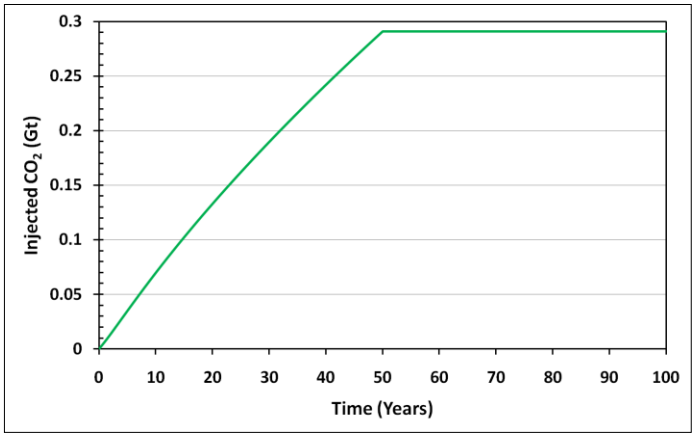

Figure 16: Injection capacity for object-based modelling.

Based on this limited number of realizations, it is possible to suggest that the small (compared to plume size) scale heterogeneity considered in this study does not play a strong role for pressure and saturation fields and for overall capacity of the injection site. For layered systems and for objects comparable to plume size it will be significant, especially by selective placement of injectors. Such a study would require more detailed knowledge of the distribution properties within the aquifer.

2. LONG-TERM FATE OF CO_2

In this section, we discuss the long-term fate associated with the following phenomenon:

- Increased aquifer pressure during and after injection.
- Migration of CO_2 beyond injection area due to dip.
- Buoyant phase of CO_2 over long periods of time.

2.1. Pressure Field Evolution During and After Injection Until Initial Reservoir Pressure Reached

As discussed in previous sections, the pressure in the aquifer (within and around the injection area) will increase during the injection period and then gradually decrease to the initial pressure distribution, due to the very large volume in the Nisku aquifer. It is important to know how long it will take for a substantial pressure disturbance to dissipate. The simulation results of a 10-well scenario are presented in Figure 17.

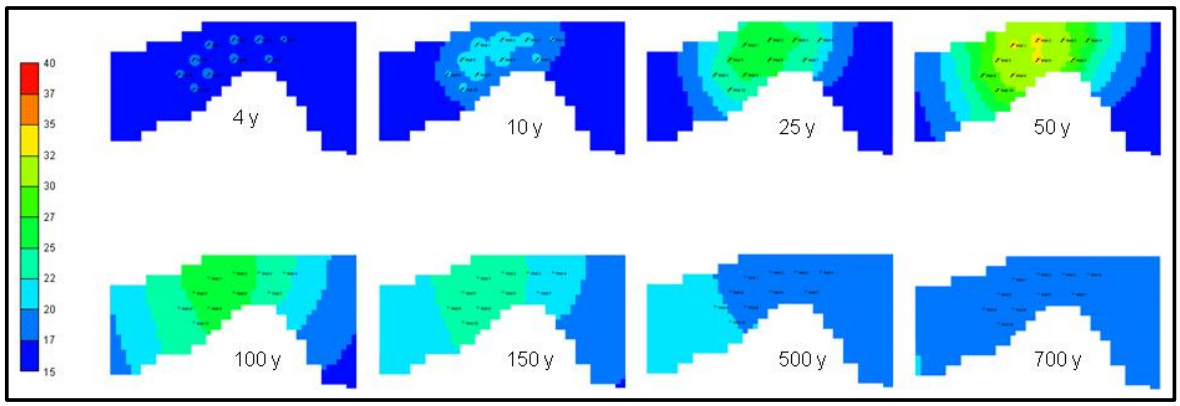

Figure 17: Pressure evolution (each well injects 0.5 Mt/year for 50 years).

One can see that the pressure does not reach initial reservoir pressure (P_i = 16 MPa) even 650 years after injection stops, although the difference in ΔP is small compared to the maximum difference (ΔP_{max}=24 MPa = P_f-P_i at the end of injection). The graph of ΔP versus time is presented in Figure 18, which allows for estimating the timescale of pressure decay.

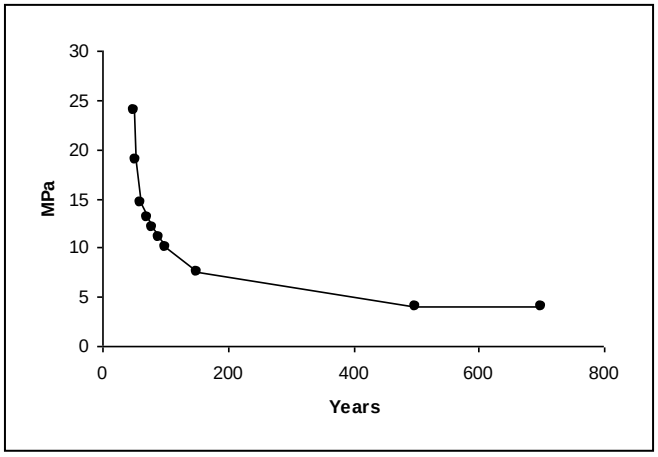

Figure 18: ΔP versus time.

From this graph (assuming exponential behavior), ΔP falls *e (~ 2.7)* times at ~ 120 years, thereby providing the timescale of high pressure fate for injection design.

2.2. Effect of Aquifer Dip on Plume Movement and Size

The effect of aquifer dip was evaluated by simulations using the base Nisku properties (Figure 4) for single-well injection at a rate of 1 Mt/year for 50 years. Simulations run up to 1000 years after injection started and two cases were considered for comparison: i) dip = 0 and ii) dip = 0.5°. The results of CO_2 saturation at the top layer versus time are shown in Figure 19. One can see that at base conditions the effect of dip on the plume movement is marginal (Figure 19-a), although when permeability was increased (while all other parameters remained the same) noticeable plume migration along the dip was observed (Figure 19-b).

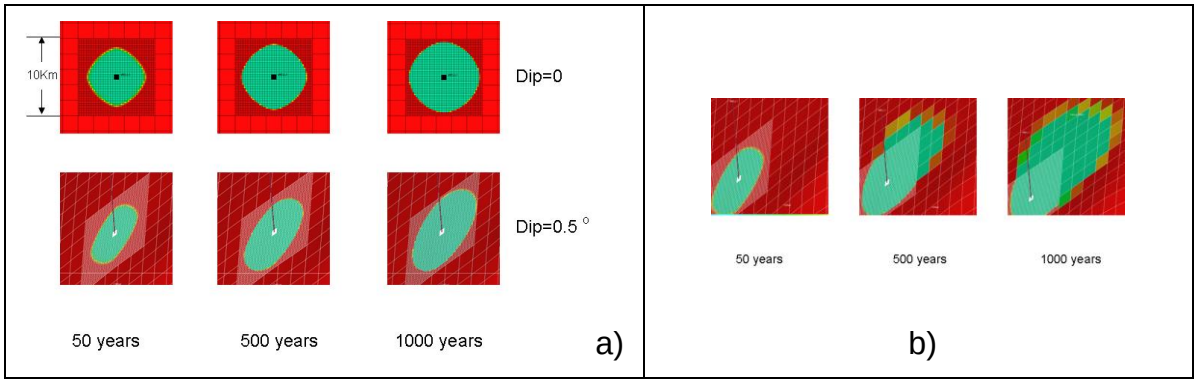

Figure 19: Saturation field for a single injector: a) base properties; b) permeability is increased to 150 mD.

What this means is if the plume reaches regions with higher permeability, it will migrate upwards and this should be taken into consideration.

2.3. Estimation of Timescale for Free-Phase CO_2 after Injection (onset and dissolution time for natural convection scenario)

The CO_2 injected into a deep aquifer is typically 10 to 40% less dense than the resident brine. Driven by density contrasts, CO_2 will first flow vertically and then horizontally spread under the caprock. If there are breaches in the caprock, leakage could occur through these high permeability zones or through artificial penetrations, such as abandoned wells. It is very important to know how long free-phase CO_2 remains in the reservoir and how long complete dissolution of CO_2 into the brine takes because this determines the time that free-phase CO_2 has to leak from the formation. After injection, free-phase CO_2 (gas or supercritical fluid) will be partially trapped as residual saturation and the remainder will slowly dissolve in the brine *[8]*. Depending on reservoir properties, different mechanisms may be responsible for dissolution. In this section we estimated the dissolution mechanisms for the Nisku conditions and associated timescale of dissolution. The analysis is based on Hassanzadeh et al, 2007 *[9]*. In the short term (Figure 20 a), during and after injection, some amount of CO_2 is residually trapped and the remainder may be dissolved by natural convection (Figure 20 b). First, we found convective mechanisms in the Nisku aquifer or at Nisku conditions, then we estimated the onset of natural convection and the corresponding timescale.

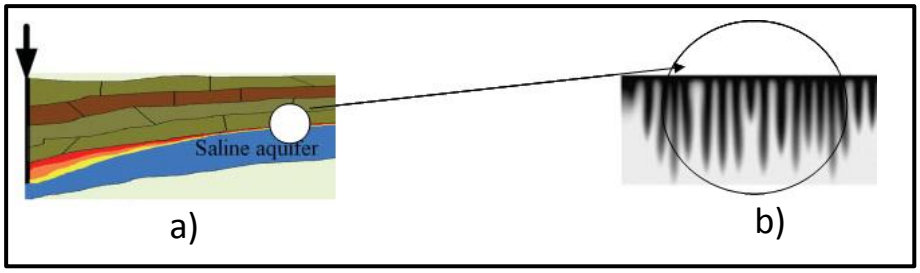

Figure 20: Short-term (a) and long-term (b) processes involved in geological storage.

The important parameter to describe the stability of such a system is the porous medium Rayleigh number. It is defined by

$$Ra = \frac{k g \Delta\rho H}{\mu \phi D}$$

where

k is permeability,

ϕ is porosity,

g is acceleration due to gravity,

H is aquifer thickness,

μ is viscosity,

$\Delta\rho$ is the density difference (CO_2 saturated and fresh brine), and

D is the molecular diffusion coefficient.

If Ra > 49 — natural convection occurs, Hassanzadeh et al, 2007 *[9]*. For the Nisku conditions, Ra is ~ 400 from which we estimated the onset of convection at these conditions (t_{onset} ~ 80 years) and timescale of convective dissolution (T_{dis} ~ 3000 years). Estimations are made based on Hassanzadeh et al, 2007 *[9]*.

3. INVESTIGATION OF THE PHASE BEHAVIOR OF H_2S SATURATED BRINE IN CO_2 SEQUESTRATION PROCESS

It was found (see the Geochemistry section of this report) that the Nisku brine includes dissolved H_2S. The folloing section investigates the behavior of H_2S during the CO_2 sequestration process.

3.1. Fluid Representation of CO_2-Brine and CO_2-H_2S-Brine Systems

The solubility of gaseous components in the aqueous phase in CMG-GEM *[10]* is modelled by employing Henry's law. The fugacity of components is calculated using the Peng-Robinson Equation-of-State. GEM version 2008.12 uses accurate models for the Henry's constants of CO_2 and H_2S taking into account pressure, temperature and salinity (salting-out coefficient) by Harvey semi-empirical correlation *[11]*. At initial condition of the Nisku formation (pressure = 16 MPa, temperature = 60°C, and salinity = 190,000 mg/litre), the CMG calculates the concentration of dissolved H_2S in a saturated brine equal to 0.023 by mole fraction in the aqueous phase, which

aligns with the value reported in the literature, Duan et al, 2007 *[12]*. For calculating the viscosity and density of the aqueous phase, Kestin's *[13]* and Rowe's *[14]* correlation were used respectively.

3.2. Description of the Simulation Model

Since the focus of this study was to investigate the fate of existing H_2S in the Nisku formation during CO_2 injection, the simulation was limited to a single well located at the centre of a bounded radial model with a production well at the boundary to mimic a constant pressure boundary condition. Therefore, simulations were performed in a one-dimensional radial (r x z = 1) model with the total extend: radius of 500 m and a net aquifer thickness of 5 m. The absolute permeability and porosity of the model were equal to 2000 md and 0.3, respectively to allow proper propagation of CO_2 plume after a few days. With respect to initial concentration of dissolved H_2S, two cases were considered. In the first case the initial mole fraction of dissolved H_2S was taken as 0.02; and in the second case as 0.005 (the balance being water).

Limited information about the relative permeability curves encouraged us to use the Corey correlation *[15]* with exponents of 2.0 and 1.5 for the gas and water relative permeability curves. Figure 21 shows the relative permeability data for gas and brine. The residual brine saturation was set equal to 0.1 and two different end points show relative permeability values for the gas phase as 0.4 and 1.0. These were considered for the base case and one for sensitivity analysis respectively. Pure CO_2 at supercritical conditions was injected for 200 days at a rate equal to 5000 SM^3/day.

The effect of discritization on solution accuracy was investigated by conducting simulations with 500 × 1, 1000 × 1, 2000 × 1 grid block systems. The simulation model with a 500 × 1 resolution was not sufficiently accurate. But the comparison of results indicated that the 1000 × 1 produced results within 5% of the 2000 × 1 resolution, indicating that discritization errors become negligible at or above the 1000 × 1 resolution.

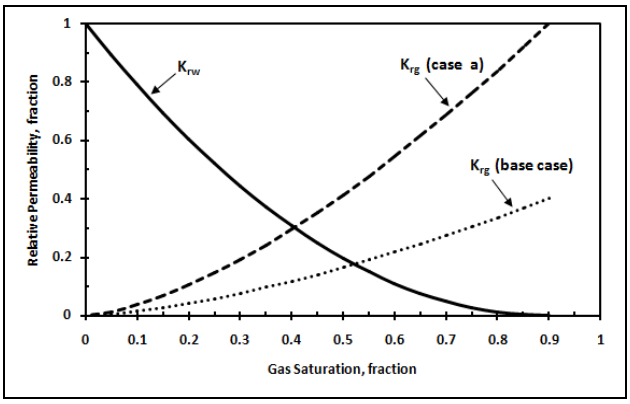

Figure 21: Water-gas relative permeability curves.

3.3. General Simulation Results

The preliminary simulation results presented below indicate that injection of pure CO_2 into a saline aquifer that contains measurable concentrations of dissolved H_2S causes the vaporization and release of dissolved H_2S into the expanding CO_2 plume. Moreover, the expanding CO_2 plume progressively delivers all of the vaporized H_2S towards the leading edge of the plume. Figure 22 shows the gas saturation variation within the aquifer after 200 days.

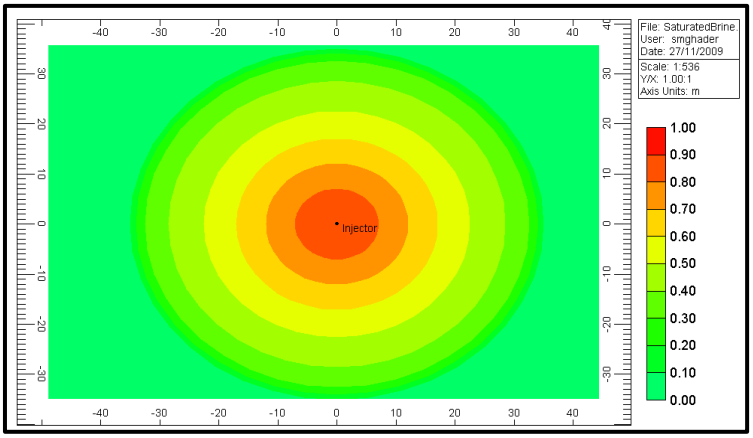

Figure 22: Variation of gas saturation around the injection well after 200 days.

As shown in Figure 23, the mole fraction of CO_2 within this plume changes from 1.0 at the point of injection and gradually decreases toward zero close to the outer boundary of the plume.

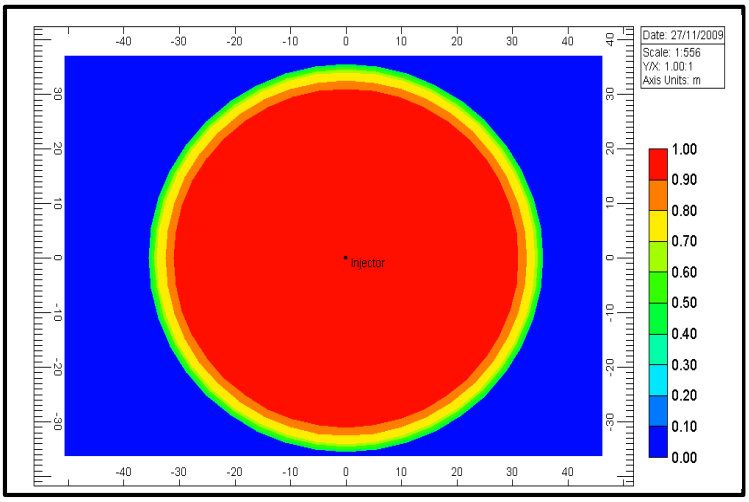

Figure 23: Variation of CO_2 mole fraction ($y^v_{CO_2}$) in the gas phase after 200 days of CO_2 injection. Note that the mole fraction of H_2S ($y^v_{H_2S}$) at any location is equal to $1.0 - y^v_{CO_2}$.

Figure 24 illustrates the variation in the composition of the plume after 200 days as a side view.

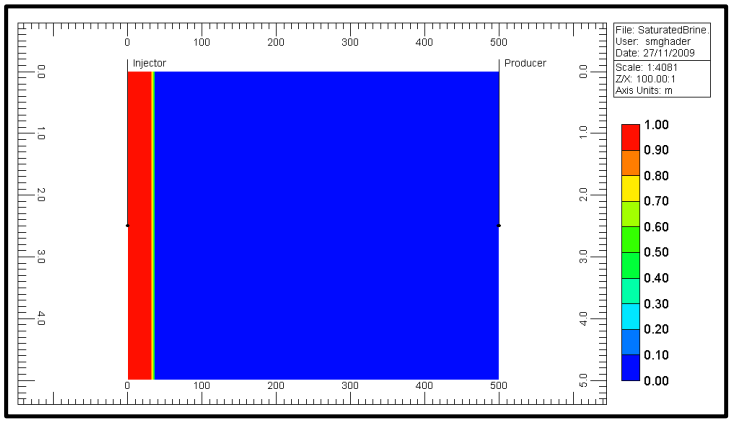

Figure 24: Side view of the variation of CO_2 mole fraction in the gas phase after 200 days. This figure also shows the position of the production well.

Since the plume expansion is symmetrical in the radial models, it is reasonable to use 2D graphs to better illustrate the development of gas saturation and H_2S evolution as the vaporizing gas drive progresses.

3.4. Base Case Simulation Results and Observations

As suggested by the above grid sensitivity results, a discretization of 1000×1 (r $\times$ z) was chosen as the base case and explored to investigate the consequences of injecting CO_2 into a brine saturated with (dissolved) H_2S at initial conditions. For the base case scenario, pure CO_2 is injected at a rate of 5000 RSM^3/day for 200 days into a vertical well located at the centre of the domain. As previously described, when the injected CO_2 comes into contact with the brine, H_2S progressively vaporizes out of the aqueous phase into the gas phase of the advancing CO_2 plume. The CO_2 plume pushes the mobile portion of the brine, as well as the vaporized H_2S, toward the outer boundary of the domain while the CO_2 continuously dissolves into the residual brine.

Therefore after the start of CO_2 injection, the region swept by the plume consists of two sub-regions. An inner radial sub-region extending from the injection well is characterized by the absence of H_2S in the aqueous phase. In fact, the dissolved H_2S in this inner sub-region is nearly completely removed from the brine via this vaporizing gas process. The second sub-region extends from the outer edge of the inner sub-region to the leading edge of the plume. In this outer sub-region, the concentration of H_2S in the CO_2 plume gradually increases toward an upper boundary and sometimes reaches a significantly high concentration at the leading edge of the plume. From Figure 25, it is inferred that for the base case scenario and after 200 days, the plume radius will be approximately 35.5 m, of which 27 m belong to first sub-region and the remaining 8.5 m is considered to be the second sub-region.

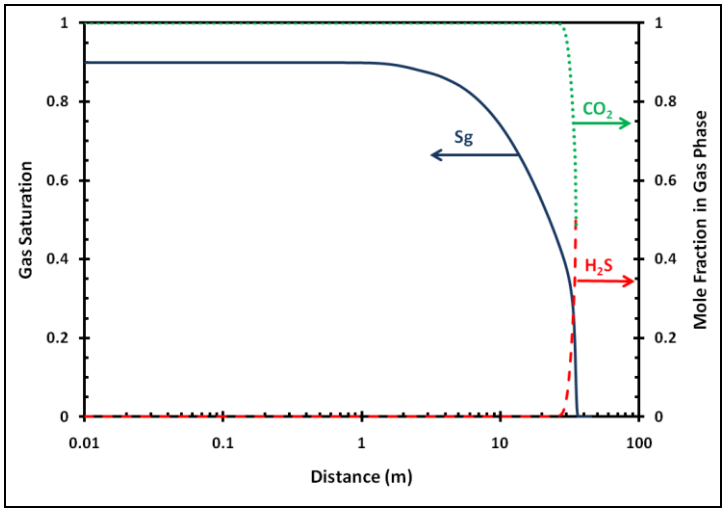

Figure 25: Distribution of different phases and components within the aquifer after 200 days. Midnight blue solid curve: variation of gas saturation versus distance around the injection well, residual brine saturation is equal to 0.1. Green dotted curve: variation of CO_2 mole fraction in the gas phase. Red dashed curve: variation of H_2S mole fraction in the gas phase.

Figure 26 clearly shows that the CO_2 has been dissolved into the immobile portion of the brine, while H_2S has been vaporized and released into the gas phase.

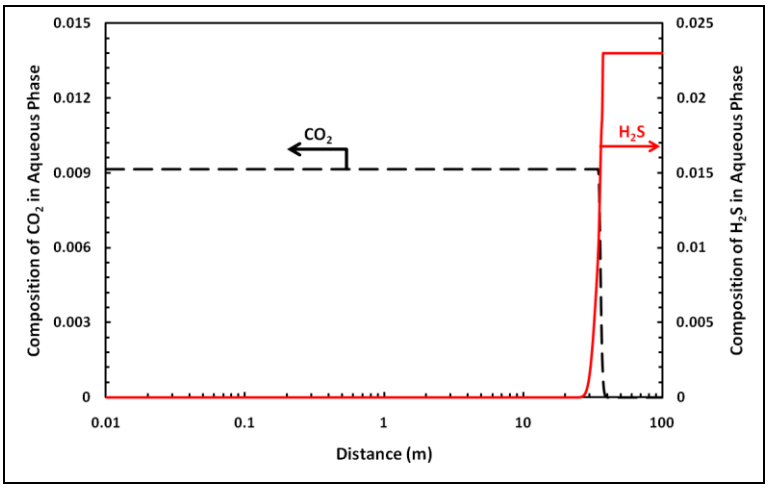

Figure 26: Composition of the aqueous phase in the region swept by the plume after 200 days. Note that the position at which the CO_2 mole fraction reaches zero coincides with the outer edge of the plume, after which the water (brine) saturation is equal to one.

3.5. Sensitivity Analysis

Simulations were conducted to investigate the effect that flow conditions have on the distribution of different phases and components, and specifically the evolution of H_2S at the leading edge of the plume. For simplicity, the results after 200 days of injection are presented. Flow conditions are affected by gas solubility, gas mobility, and initial H_2S saturation in the brine with respect to the aqueous phase. The results are illustrated in Figure 27.

(a) Effect of Gas Solubility

The effect of solubility was examined by considering pure water instead of brine. It was assumed that the initial concentration of H_2S was equal to the saturated brine base case. The higher solubility of the non-hydrocarbon components into the pure water relative to the brine case causes the ultimate radius of the CO_2 plume to shrink, from 35.5 to 34.5 m in the base case. This indicates less H_2S was released from the (sour) pure water case (see Figure 27-a).

(b) Effect of Gas Mobility

The effect of gas mobility was examined by changing the gas relative permeability and increasing the end point of gas permeability from 0.4 to 1.0 (Figure 1, K_{rg} [case a]). In the case of a more adverse mobility ratio (higher gas mobility), the gas spread over a larger contact area with the aqueous phase (larger radius of plume equalled 42 m), thereby more effectively stripping H_2S away from the brine when in contact with the advancing gas front (see Figure 27-b).

(c) Effect of Initial Concentration of Dissolved H_2S in Brine

Simulations were run for another case where the initial concentration of the dissolved H_2S in the brine was decreased by 25%. Hence, in this case the initial mole fraction of H_2S in the brine was equal to 0.005. The simulation results in Figures 27-c revealed that although the cumulative mass of released H_2S (determined by calculating the area under the graph of H_2S concentration versus distance) is reduced by decreasing the initial concentration of the dissolved H_2S in brine, the mole fraction of released H_2S in the gas phase is still high. These results also illustrate the fact that the initial concentration of H_2S has a second-order effect on the evolution of H_2S during CO_2 sequestration.

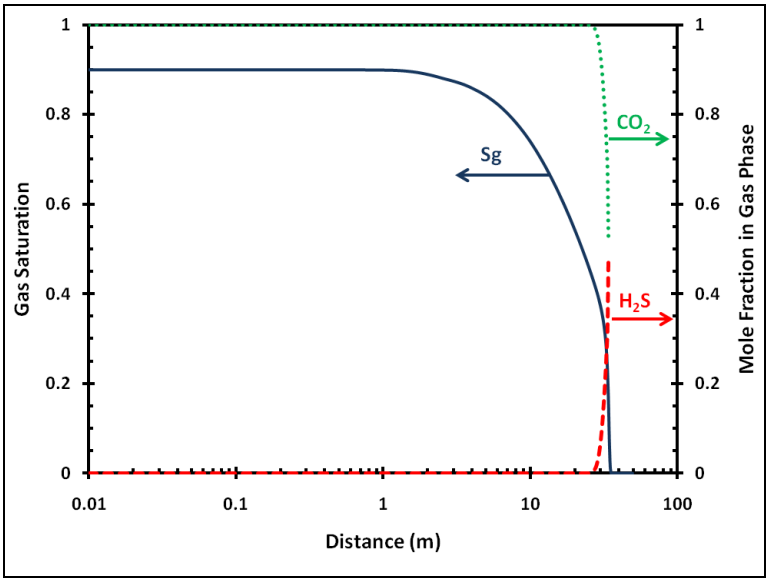

(a)

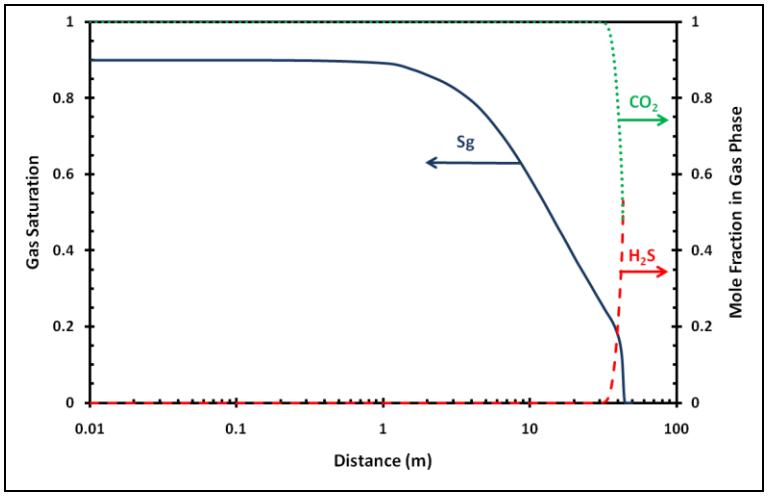

(b)

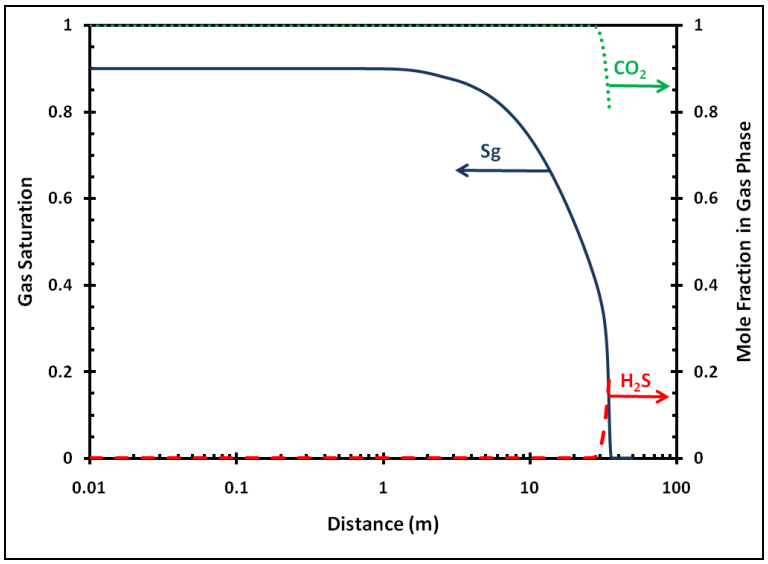

(c)

Figure 27: Effect of different parameters on the distribution of different phases and components beneath the caprock after 200 days: (a) increased gas solubility, (b) increased gas mobility, (c) decreased initial mole fraction of dissolved H_2S in the brine by 25%.

SUMMARY

In this study, we performed numerical modelling of injecting large volumes of CO_2 (1 Gt target over 50 years) into the Nisku Formation. Injection was performed within localized injection areas of 30 km × 60 km. The main objectives of the study were to:

- estimate the injection capacity and CO_2 plume movement and pressure distribution during and after injection;
- estimate the timescales of the long-term fate of injection associated with free-phase CO_2, aquifer pressurization, and the effect of dip on plume shape and migration; and
- assess possible H_2S concentration (mole fraction) in the CO_2 plume over time and space.

It was shown that the capacity of injection is limited not by available pore space, but by the ability to inject without exceeding the fracture pressure of the formation. Although capacity increases with the number of injectors, increasing the number of wells has a limit. Very strong interference between pressure plumes was observed with no substantial benefit beyond 20 wells. Horizontal injection wells and aquifer fracturing may be considered as options to increase capacity. Sensitivity of capacity to reservoir permeability, rock compressibility and well placement was investigated.

The saturation and pressure field simulations show that for multiple injection scenarios (*n* wells), CO_2 saturation plumes have no interference; we see *n* individual plumes with a radius of 4 to 5 km for each injector. The pressure field behaves completely different than the saturation field. There are no individual pressure plumes, but a single large (scale of hundred km) pressure disturbance.

It was shown that the dip in the Nisku formation does not affect the results (i.e., no substantial plume movement), although free-phase CO_2 may migrate along the dip if it reaches a zone with higher permeability (above 100 mD). We estimated that at the Nisku conditions, the timescale for pressure decay is 120 years and the timescale for free-phase CO_2 dissolution is ~ 3000 years where the mechanism of dissolution is natural convection.

An assessment of the possible H_2S concentrations in the CO_2 plume over time and space was performed. It showed that H_2S dissolved in aquifer brine will be released into the CO_2 plume during injection and will reach a high mole fraction at the outer edge of the CO_2 plume.

ACKNOWLEDGMENTS

Financial support for this work was provided by NSERC Strategic Grant and AERI, with additional funding from industry partners through the Wabamun Area CO_2 Sequestration Project (WASP) led by the University of Calgary. Simulation software (GEM) was donated by the Computer Modelling Group. This support is gratefully acknowledged. We also wish to thank Long Neighem and Vijay Shrivastava for their help with the new version of GEM and for the useful discussions of its applications to this study.

REFERENCES

[1] B. Hitchon, Aquifer Disposal of Carbon Dioxide, Hydrodynamic and Mineral Trapping – Proof of Concept, 1996, Geoscience Publishing Ltd., Sherwood Park, Alberta, Canada.

[2] H. Hassanzadeh, M. Pooladi-Darvish, A. M. Elsharkawy, D. W. Keith, Y. Leonenko, Predicting PVT data for CO_2-brine mixtures for black-oil simulation of CO_2 geological storage. Int. J. Greenhouse Gas Control, 2008, 2, p. 65–77.

[3] B. Bennion, S. Bachu, Relative permeability characteristics for supercritical CO_2 displacing water in a variety of potential sequestration zones in the western Canada sedimentary basin, Paper SPE 95547 at SPE Annual Technical Conference an Exhibition, Dallas, TX, p. 9–12 October, 2005.

[4] K. Pruess, J. Garcia, T. Kovscek, C. Oldenburg, J. Rutqvist, C. Steefel, T. F. Xu, Code intercomparison builds confidence in numerical simulation models for geologic disposal of CO_2, Energy. 2004, 29, p. 1431–1444.

[5] J. M. Nordbotten, M. A. Celia, and S. Bachu, Injection and storage of CO_2 in deep saline aquifers: Analytical solution for CO_2 plume evolution during injection. Transport in Porous Media 2005, 58(3), p. 339–360.

[6] A. Lucier and M. Zoback, Assessing the economic feasibility of regional deep saline aquifer CO_2 injection and storage: A geomechanics-based workflow applied to the Rose Run sandstone in Eastern Ohio, USA. Int. J. Greenhouse Gas Control, 2008, 2, p. 230–247.

[7] Y. Leonenko and D. W. Keith, Reservoir engineering to accelerate the dissolution of CO_2 stored in aquifers, Environmental Science and Technology, 2008, 42(8), p. 2742–2747.

[8] Hassanzadeh, H.; Pooladi-Darvish, M.; Keith, D. W. Stability of a fluid in a horizontal saturated porous layer: effect of non-linear concentration profile, initial, and boundary conditions. Transport in Porous Media, 2006, 65, p. 193–211.

[9] Hassan Hassanzadeh, Mehran Pooladi-Darvish, and David W. Keith, Scaling Behavior of Convective Mixing, with Application to Geological Storage of CO_2, AIChE, 2007, Vol. 53, No. 5, p. 1121–1131.

[10] Nghiem, L.; Sammon, P.; Grabenstetter, J.; Ohkuma, H. Modelling CO_2 Storage in Aquifers with a Fully-Coupled Geochemical EOS Compositional Simulator, SPE Paper No. 89474, 2004.

[11] Harvey, A.H. 1996. Semiempirical correlation for Henry's constants over large temperature ranges, AIChE J, Vol. 42, No. 5, p. 1491–1494.

[12] Duan, Z., Sun, R. Liu, R. and Zhu, C., 2007. Accurate thermodynamic model for the calculation of H_2S solubility in pure water and brine. Energy and Fuels, 21, p. 2056–2065.

[13] Kestin, J., Khalifa, H.E., Correia, R.J., 1981. Tables of the dynamic and kinematic viscosity of aqueous NaCl solutions in the temperature range 20–150°C and pressure range 0.1−35 MPa. J. Phys. Chem. Ref. Data, Vol. 10, p. 71–87.

[14] Rowe, A.M., Chou, J.C.S., 1970. Pressure-volume-temperature-concentration relation of aqueous NaCl solutions. J. Chem. Eng. Data, Vol. 15, 1970, p. 61–66.

[15] Corey, A.T., 1954. The interrelation between gas and oil relative permeabilities. Producers Monthly, November, p. 38–41.